MDPI

Article

Low Temperature Transitional Aluminas: Structure Specifics and Related X-ray Diffraction Features

Dmitriy A. Yatsenko *, Vera P. Pakharukova and Sergey V. Tsybulya

Boreskov Institute of Catalysis SB RAS, Pr. Lavrentieva 5, 630090 Novosibirsk, Russia;
verapakh@catalysis.ru (V.P.P.); tsybulya@catalysis.ru (S.V.T.)
* Correspondence: yatsenko@catalysis.ru

Abstract: Despite the fact that metastable aluminum oxides are actively used in industry, there is a discrepancy in the literature regarding their crystal structure. All this leads to difficulties in data interpretation and, as a consequence, classification problems. This work is aimed at solving these tasks. The main features of powder X-ray diffraction of typical samples of three Al_2O_3 polymorphs (γ-, χ-, η-) are analyzed. Specifics and fundamental differences in X-ray scattering and their relationship with the structural organization at the nanostructure level are clearly shown. The work demonstrates the possibilities of analyzing experimental powder X-ray diffraction data using a modern approach based on the Debye Scattering Equation for studying the organization of such complex systems.

Keywords: 3D nanostructure; metastable aluminum oxides; XRD; Debye Scattering Equation; planar defects

1. Introduction

Metastable alumina phases are extremely important technological materials. They are highly dispersed materials with a high specific surface area and pronounced acid-base surface properties. This leads to the widespread use of them as catalysts, carriers for catalysts and adsorbents [1–9]. A variety of metastable polymorphs makes it possible to vary widely the structure and, consequently, the properties of the materials obtained. At the same time, a large number of factors affect the features of structure formation: precursors, trace impurities, temperature and time of calcination, etc. The metastable aluminum oxides are transitional phases formed at calcination of aluminum hydroxides at temperatures insufficient for the formation of a stable corundum phase α-Al_2O_3 [10,11] (Table 1).

Table 1. The solid-state transformations of aluminum hydroxides and aluminas at different temperatures.

Temperature, °C													
0	100	200	300	400	500	600	700	800	900	1000	1100	1200	1300
Bayerite Al(OH)$_3$					η					θ		α-Al$_2$O$_3$	
Boehmite AlOOH					γ			δ			θ		α-Al$_2$O$_3$
Gibbsite Al(OH)$_3$					χ					κ		α-Al$_2$O$_3$	

This work is focused on the low-temperature η-, γ- and χ-Al_2O_3 polymorphs (formed at 500–850 °C). Their unique physicochemical properties are determined by the fact that they exist only in the nanocrystalline state.

It is necessary to have fundamental knowledge of not only their structure but also nanostructure for the targeted synthesis of new materials and control of functionally important characteristics.

X-ray powder diffraction is the main tool for the qualitative differentiation of three-dimensionally ordered phases because it is sensitive to differences in the crystal structure of the compounds under study. In addition to the standard X-ray diffraction (XRD) analysis,

the main criteria for differentiating the low-temperature Al_2O_3 polymorphs are also such diffraction features as the kind of anisotropic broadening of peaks, changes in their profile or the appearance of additional diffuse scattering. The reason is that the nanoparticles of transitional Al_2O_3 phases exhibit planar structural defects and are composed of crystallites of several nanometers in size. Standard methods of XRD phase analysis and crystal structure refinement based on the concepts of Bragg diffraction (the Rietveld method, etc.) are not applicable for such objects.

The crystal structure of the low-temperature polymorphs (γ-, η-Al_2O_3) is usually described within the framework of a unified structural model of nonstoichiometric spinel with different distribution of cations over octahedral and tetrahedral positions [11–15]. The structure of χ-Al_2O_3 polymorph has been studied to the least degree, there is no unambiguous opinion even about the symmetry group of the crystal lattice [11].

However, it is well known that the standard crystallographic model cannot describe the distinctive features of powder XRD patterns associated with the presence of diffuse scattering due to crystal structure disorder.

The work [16] became the starting point of a new concept of the structure of the metastable Al_2O_3 polymorphs. The concept is based not on differences in the crystal structure parameters (distribution of cations over cationic positions), but on the specifics of particle nanostructure: the polymorph of primary nanoscale crystal blocks, ways of their stacking along different faces. Notice that the nanoparticle topology is determinant for the mechanical properties of nanomaterials [17,18]. Analysis of the effects of planar defects in different crystallographic planes on diffraction was performed based on simulation of XRD profiles for statistical model of a one-dimensional (1D) disordered crystal with taking into account electron microscopy data [16].

However, the 3D nanostructures could not be checked by used approach for simulation of powder XRD patterns from 1D disordered crystal. Further study of the nanostructure of the low-temperature Al_2O_3 polymorphs was suspended due to the lack of tools for modeling the 3D nanostructure of particles and verifying the models for compliance with experimental diffraction data. We have recently proposed to use a method for calculating diffraction patterns from atomic models of 3D nanostructures using the Debye Scattering Equation (DSE). A model of a coherent 3D nanostructure of anisotropic particles of the tetragonal modification of γ-Al_2O_3, which adequately describes the experimental powder X-ray diffraction pattern, was first proposed by us [19]. Later, Rudolph et al. reported a study of γ-Al_2O_3 oxide for the presence of antiphase boundaries and nanostructuring, which was also performed with the use of DSE [20].

For other low-temperature polymorphs of aluminum oxide, such 3D models of the nanostructure are still missing. For their construction in the future, it is necessary to perform some preliminary analysis of the reproducible characteristic features of X-ray powder diffraction patterns of the different Al_2O_3 polymorphs. As a basic tool, an original approach was used to generate atomic models of 3D nanostructured Al_2O_3 particles, to calculate corresponding diffraction patterns with use of DSE and to compare of the calculated XRD profiles with experimental ones.

Briefly, there are considerable discrepancies in the literature concerning the crystal structure of the different low temperature Al_2O_3 polymorphs that leads to significant difficulties and mistakes in interpretation of the diffraction data. In this work, we demonstrate how the features of formation of 3D nanostructures lead to characteristic diffraction effects. Description of these diffraction effects allows one to solve problem of unambiguous identification and classification of the metastable Al_2O_3 polymorphs on the base of diffraction data.

2. Materials and Methods

The samples were obtained by dehydration of the corresponding hydroxide precursors, i.e., the γ-Al_2O_3 polymorph was obtained from boehmite (pseudoboehmite), η-Al_2O_3 from

bayerite, χ-Al$_2$O$_3$ from gibbsite (600 °C, 4 h). More details of the preparation procedure can be found elsewhere [16,21,22].

The experimental X-ray powder diffraction patterns were obtained on a X'TRA diffractometer (Switzerland). The data were obtained in the range of 10–75° with a step of 0.1° in 2θ (accumulation time per point was 10 s) at the CuKα radiation wavelength (average λ = 0.15418 nm), tube current 35 mA, voltage 40 kV.

2.1. Basic Crystallographic Model of the Structure

The structure of metastable phases of aluminum oxide is considered on the basis of a defective (nonstoichiometric) spinel structure with a distribution of cations over octahedral and tetrahedral positions [13,16,23–28].

The spinel cubic structure of the **AB$_2$O$_4$** compounds is described in a space group $Fd\bar{3}m$ (fcc lattice) where oxygen anions form a cubic close packing (Figure 1). **A** cations occupy tetrahedral positions (8a) and **B** cations occupy octahedral positions (16d). In an ideal spinel structure, cation **A** is divalent, cation **B** is trivalent, so the ratio of cations and anions is 3:4.
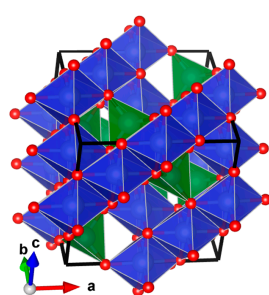

Atom		Position	Coordinates	Occupancy
	A	octahedral 16d	1/2, 1/2, 1/2	0.83
	B	tetrahedral 8a	1/8, 1/8, 1/8	1
	O	close packing 32e	1/4, 1/4, 1/4	1

Figure 1. Unit cell of the **AB$_2$O$_4$** spinel structure used for calculations (rendered in the Vesta program [29]).

In the case of aluminum oxide having cations only in the oxidation state 3+, the stoichiometric ratio is 2:3. Vacancies should appear in the cation sublattice of the spinel structure type since the stoichiometric ratio is 2.67:4. An important issue is the distribution of the vacancies. Thus, some authors give preference to vacancies in the tetrahedral positions [24,25], while others believe that the vacancies are located in the octahedral positions [26,27] or have some distribution over the both positions. Moreover, several authors assume the presence of "non-spinel" cationic positions of tetrahedral **A*** (8b) and octahedral **B*** (16c) types [13,23,30]. Until now, there is no consensus on how the vacancies are located: statistically or orderly.

The parameters of the crystallographic model of Al$_2$O$_3$ structure used for our calculations of diffraction patterns are given in Figure 1.

2.2. Modeling Technique

In this work, features of diffraction patterns of the low-temperature Al$_2$O$_3$ polymorphs will be considered from the concept of their structural organization as coherent nanostructures [16], consisting of crystalline blocks of certain morphology stacked coherently along certain crystallographic faces.

It is impossible to determine planar defects violating the conditions of Bragg diffraction with use of standard XRD methods. They appear as diffuse scattering of X-rays, which requires the use of special analytical approaches. To analyze diffraction effects at the work [16] the method for calculating X-ray scattering for 1D disordered objects was used [31,32]. However, this method does not allow one to calculate the complete diffraction patterns for 3D nanostructures, since it does not make it possible to stack simultaneously the crystal blocks in three different crystallographic directions.

As mentioned above, we have demonstrated the fundamental possibility of calculating diffraction patterns from 3D models of nanostructured particles by the Debye scattering equation (DSE) [33–35] by the example of γ-Al_2O_3 [19]. The method allows calculating the full XRD profiles from any set of atoms using the relationship of X-ray scattering with interatomic distances within the kinematic theory. It is applicable to any structure including non-crystalline and nanostructured materials. The intensity values are calculated at each point of the diffraction pattern (not only at Bragg angles) with taking into account diffuse scattering and without artificial broadening of reflections in contrast to the Rietveld method. DIANNA software was used to calculate diffraction patterns by DSE (Diffraction Analysis of Nanopowders) [36]. Calculations were performed for a monochromatic CuKα wavelength $\lambda = 0.15418$ nm.

3. Results and Discussion

Comparison of the diffraction patterns of the samples with the bar diagram of reflections characteristic to spinel structure is shown in Figure 2.
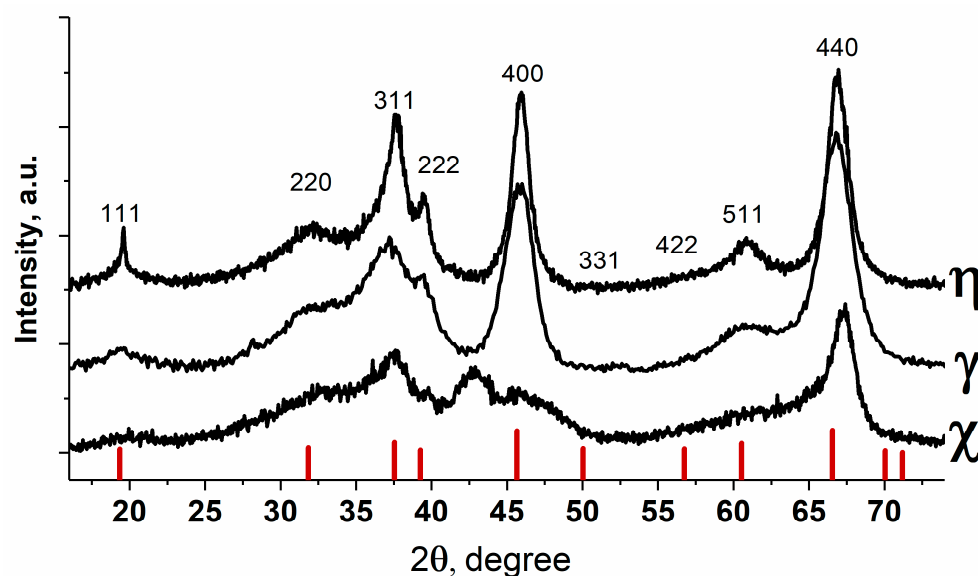

Figure 2. Experimental powder X-ray diffraction patterns of the Al_2O_3 samples [16]. Bar diagram of characteristic spinel reflections is depicted.

It can be seen that the diffraction corresponds to the spinel structure with the exception of the peak at 42.8° in 2θ (interplanar distance 0.211 nm) for χ-Al_2O_3 (Figure 2). This peak cannot be in the XRD pattern of cubic spinel. Diffraction pattern of η-Al_2O_3 differs from others in the shape and broadening of the 111 reflection.

An important feature of all the diffraction patterns of the metastable aluminum oxides is the different broadening of the peaks corresponding to the same crystallographic direction [110]. Reflection 220 is much wider than 440 and this feature indicates the presence of nanostructuring in all three polymorphs. Since the spinel structure has a cubic close packing of oxygen atoms along {111} directions, crystallites of a polyhedral shape with cut-off planes (10$\bar{1}$), ($\bar{1}$10), (111) were used for modeling. It should be noted that for different polymorphs of aluminum oxides, different shapes of crystallites were suggested [16,19]. However, in this work, in order to show the fundamental differences in the organization of nanostructures of γ, η and χ polymorphs, diffraction effects will be shown in the frame of the chosen habit.

3.1. Nanostructure-Related Diffraction Effects by the Example of γ-Al$_2$O$_3$

At the beginning, the experimental powder X-ray diffractogram of the γ-Al$_2$O$_3$ sample was described by the superposition of Pseudo-Voight functions (Figure 3) using the Fityk software [37].
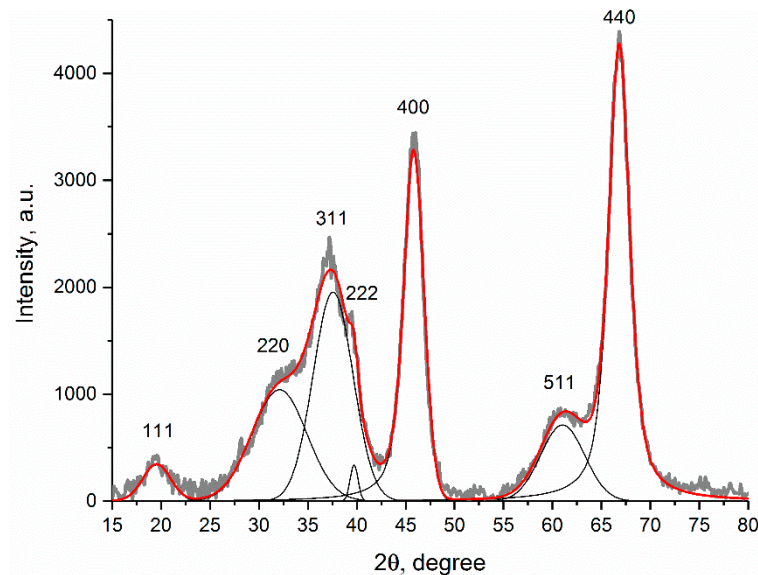

Figure 3. Decomposition of the experimental powder X-ray diffraction pattern of γ-Al$_2$O$_3$ by the Pseudo-Voight functions.

It is possible to estimate the lattice parameter (a = 0.786 nm) and the coherent scattering regions (CSR) sizes corresponding to different crystallographic directions. The CSR sizes were calculated using the Scherrer formula [38] (k = 0.9). The parameters of the described peaks are presented in Table 2.

Table 2. Parameters of the described diffraction peaks and the calculated CSR sizes.

# Peak	hkl	Center	FWHM	CSR, nm
1	111	19.56	3.3	2.4
2	220	32.11	6.6	1.3
3	311	37.58	4.8	1.7
4	222	39.73	0.9	9.0
5	400	45.78	2.5	3.5
6	511	61.03	5.3	1.7
7	440	66.81	2.6	3.7

It can be seen from the table, the reflections 220 and 440 are differently broadened despite the fact that they are reflections from the same crystallographic system of planes. Scattering by the oxygen anionic sublattice is mainly responsible for the 440 reflection (this can be estimated by analyzing the contributions of different sublattices to the corresponding structural amplitude). Hence, we can assume the presence of planar defects that violate the scattering coherence only in the cation sublattice. The broadening of the 220 and 440 reflections is described by crystallites with average size of about 1.5 and 4 nm, respectively. Diffraction patterns for crystallites with theses sizes were calculated and presented in Figure 4.
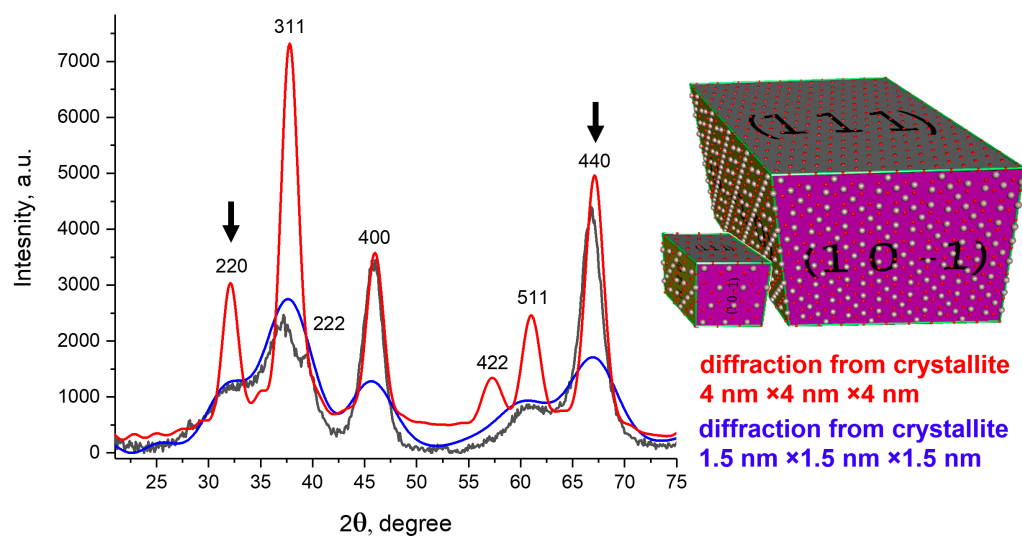
Figure 4. Experimental powder X-ray diffraction pattern in comparison with calculated diffraction patterns from crystallites with dimensions of 1.5 nm × 1.5 nm × 1.5 nm and 4 nm × 4 nm × 4 nm for γ-Al$_2$O$_3$. The arrows depict the main differences in 220 and 440 reflections.

Thus, we can conclude that there are coherently scattering regions of 1.5 and 4 nm in length. If we assume that the oxygen sublattice is responsible for CSR of 4 nm, then the 1.5 nm region can be obtained by violating the coherence in the arrangement of aluminum ions by mutual shifting the Al$_2$O$_3$ crystallites. The schematics of the displacement defect at which the anionic oxygen sublattice is retained, but the cationic one is violated, is shown in Figure 5.
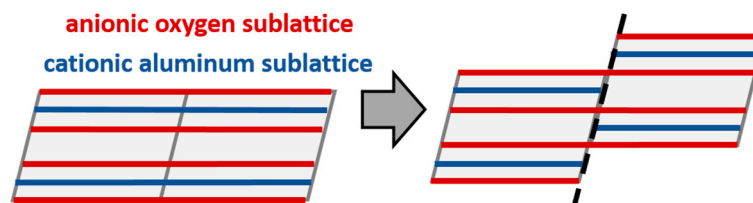

Figure 5. Schematics of modeling a planar defect with preservation of the oxygen sublattice and disruption of the cation sublattice.

A particle of 4 nm in size can be obtained from 12 blocks (nanostructure elements): 3 blocks in the [111] direction and 2 in the perpendicular direction (Figure 6). Offsetting the blocks is equivalent to reselecting the origin. Coordinates (0.25, 0.25, 0.25), (0.25, 0.75, 0.25), (0.5, 0.5, −0.25) and (0, 0.75, 0) were used as the origin in calculations.

It can be seen that the model well describes the considered diffraction effect of different broadening of 220 and 440 peaks (compare Figures 4 and 6). Since this effect is observed in the diffraction patterns of all the Al$_2$O$_3$ polymorphs under study (Figure 2), this indicates that all the Al$_2$O$_3$ samples have similar way of joining crystal blocks. The following detailed studies are required to clarify the predominant crystallographic planes along which the blocks are stacked with partially coherent interfaces.
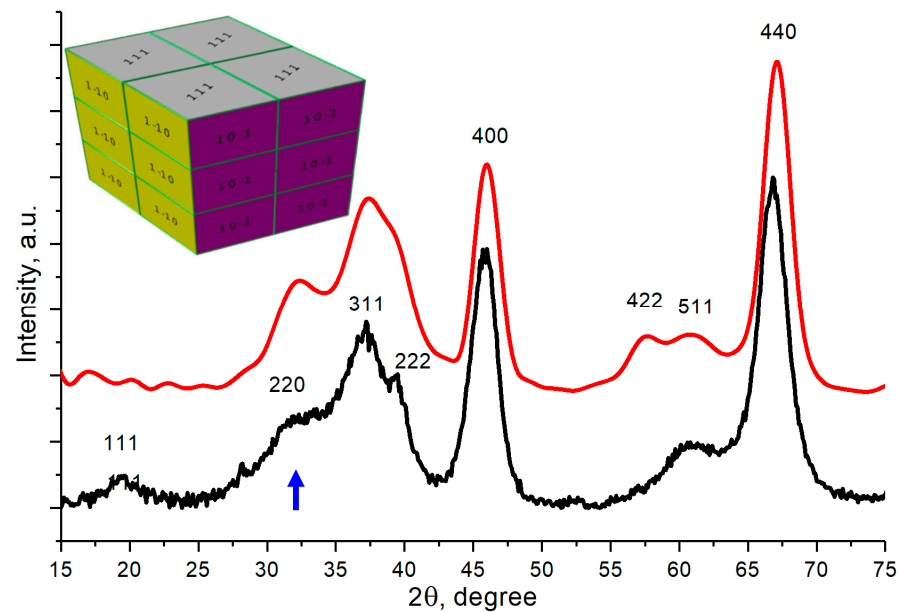
Figure 6. Experimental and calculated powder X-ray diffraction patterns from a nanostructure consisting of partially coherent 12 blocks (2 nm × 2 nm × 1.4 nm) for γ-Al$_2$O$_3$. The arrow indicates the main explained feature-broadening 220 reflection.

3.2. Diffraction Feature of χ-Al$_2$O$_3$, Which Is Not Typical for the Spinel Structure

The diffraction pattern of the χ-Al$_2$O$_3$ retains most of the features inherent in the diffraction pattern of the γ-Al$_2$O$_3$, with the exception of additional scattering at 42.8°. Dependence of the peak intensity on the synthesis conditions and the used precursors suggests that the peak is related to presence of planar defects. The authors [16,39] associated it with stacking faults in the anion sublattice of the spinel structure.

So, S.V. Tsybulya and G.N. Kryukova in [16], with use of the model of 1D disordered crystal considered structure in which the sequence of oxygen layers changed statistically, forming either hexagonal (ABABAB) or cubic (ABCABC) packing of oxygen. The results suggested that the appearance of this additional "non-spinel" peak is related to faults in anion close packing. The broadening of the 220 reflection with the preservation of the 440 width was suggested to be explained by displacement defects in the {110} planes. Indeed, our DSE calculations for atomic models of nanoparticles with different packing of oxygen atoms confirm these conclusions. If along the [111] direction we add to the crystal blocks with cubic (ABC) packing of oxygen layers, blocks with hexagonal packing (AB), a diffuse scattering peak (which is not typical for the space group Fd3m) appears in the region of 43° in 2θ (Figure 7).

The resulting model is not the best approximation, but it qualitatively shows the features of the formation of χ-Al$_2$O$_3$. This is the only polymorph of aluminum oxide in which planar defects exist not only in the cationic but also in the anionic sublattice. To describe all the features of the full diffraction profile of χ-Al$_2$O$_3$, it is necessary to go from 1D to 3D nanostructure, with joining nanocrystalline blocks along several crystallographic planes, as was demonstrated for γ-Al$_2$O$_3$. Moreover, understanding of structural factors affecting intensity of the additional peak is required. However, this will be a separate work.
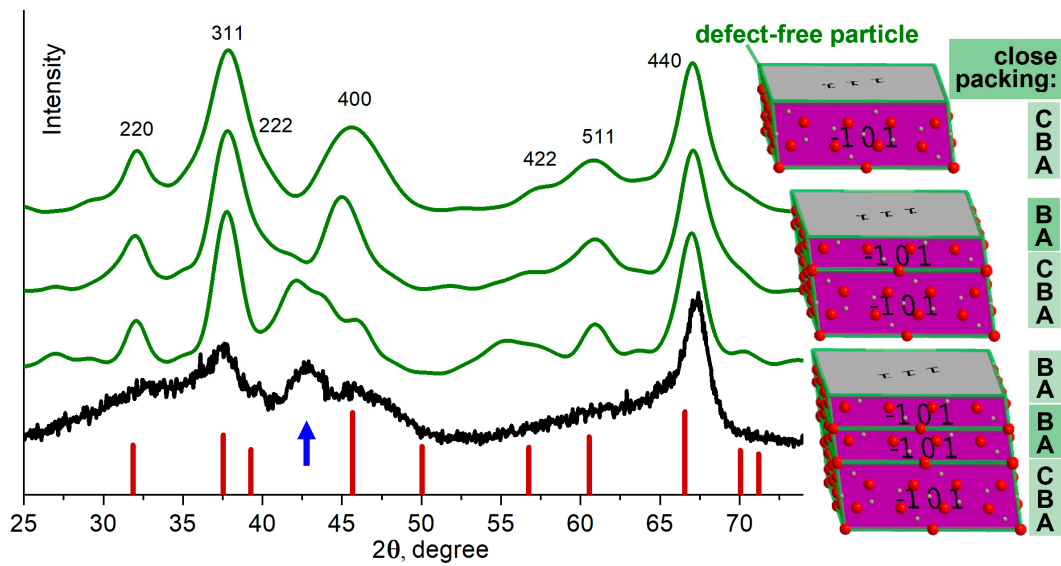
Figure 7. Experimental powder X-ray diffraction pattern of χ-Al$_2$O$_3$ and calculated diffraction profiles for models with cubic close packing ABC (2 nm × 2 nm × 0.6 nm), models assuming joining cubic with hexagonal domains ABC + AB (2 nm × 2 nm × 1.1 nm) and ABC + AB + AB (2 nm × 2 nm × 1.6 nm). The arrow indicates the main explained feature-appearance of the additional peak.

3.3. Nanostructure-Related Diffraction Features for η-Al$_2$O$_3$

The diffraction pattern of η-Al$_2$O$_3$ retains many of the features characteristic of γ-Al$_2$O$_3$, but it is characterized by an unusual shape of the 111 reflection (Figure 2). As can be seen from Figure 8, the peak represents a superposition of wide and narrow components (wide base-narrow top). It is well known that this feature is reproducible for Al$_2$O$_3$ samples obtained by dehydration of bayerite. This effect arises from the {111} plane system due to the anisotropy of the crystallite shape.
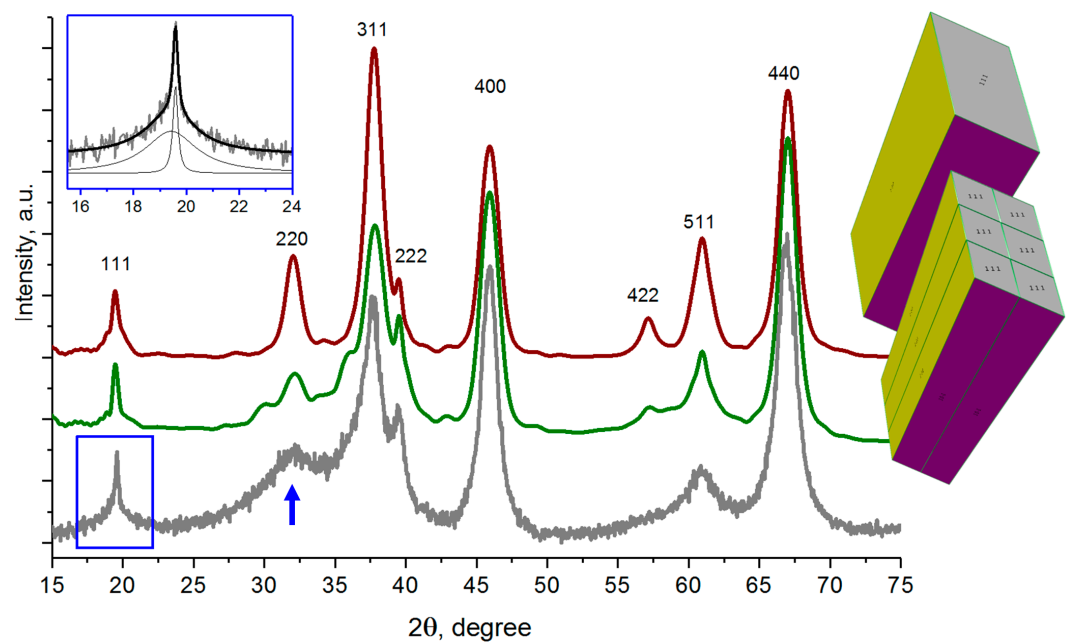
Figure 8. Experimental powder X-ray diffraction pattern of η-Al$_2$O$_3$ and calculated diffraction profiles for the model of nanostructured particle with coherent oxygen sublattice consisting of 6 blocks of 2 nm × 2 nm × 20 nm in size and model of defect-free particle of 4 nm × 6 nm × 20 nm in size. Insert-superposition of wide and narrow components of 111 reflex. The arrow indicates the broadening 220 reflection, which is caused by nanostructuring.

All 6 directions {111} are equivalent for the isotropic crystallites, the shape anisotropy violates this equivalence. According to the Scherrer formula, the narrow and wide components of the 111 reflection correspond to the CSR size of 40 and 2.5 nm, respectively. Therefore, blocks with dimensions of 2 nm $\times$ 2 nm $\times$ 20 nm elongated in the 111 direction were chosen as base elements of the nanostructure. Six staggered blocks with the origin of coordinates (0.25, 0.25, 0.25) (0, 0.75, 0) and (0.5, 0.5, -0.25) were used for the 3D nanostructure. Similarly, to γ-Al_2O_3 oxide, the observed broadening of 220 reflection was explained by planar defects leading to the nanostructuring. The resulting DSE calculations are shown in Figure 8.

It can be seen that the resulting model of nanostructured particle qualitatively describes the experiment and confirms the presence of a coherent nanostructure consisting of the elongated blocks. A more detailed description is beyond the scope of this work.

4. Conclusions

The aim of this work was to analyze the difference between the three polymorphs of the low-temperature metastable aluminum oxides (γ-, χ-, η-Al_2O_3) with regard to 3D coherent nanostructure. The main intention was to show how certain features of the 3D nanostructure lead to the appearance of reproducible characteristic features in the X-ray powder diffraction patterns. Some conclusions that can be drawn based on our calculations:

- The observed diffraction features are related to the presence of coherent nanostructures in which the primary crystalline blocks are joined to each other with maintaining the mutual orientation and parallelism of the atomic planes. All the violations of the ideal crystal structure are associated with a slip in the joining planes.
- The possibilities of DSE for determining the various nanostructures inherent in all the low-temperature Al_2O_3 polymorphs are shown.
- It is shown that the observed diffraction differences between the analyzed Al_2O_3 polymorphs are primarily associated with the peculiarities of the nanostructure (the ways of mutual joining primary crystalline blocks). The atomic structure of individual Al_2O_3 crystalline blocks corresponds to a spinel-type structure.
- The primary crystalline blocks in particles of the low-temperature Al_2O_3 polymorphs (γ-, χ-, η-) are joined in a partially coherent way with preserved atomic order in the oxygen sublattice and planar defects disrupting the cationic sublattice.
- It is shown that the characteristic peak at $2\theta \sim 42.8°$ in XRD pattern of χ-Al_2O_3 is associated with the presence of fragments (domains) with a hexagonal close packing of oxygen atoms coherently joined along the (111) planes with domains with a cubic structure.
- Primary crystallites of η-Al_2O_3 have an anisotropic acicular shape due to their larger size in the preferred direction [111].

The obtained data are useful for accurate classification of the low-temperature Al_2O_3 polymorphs on the base of diffraction data. The elaborated models are rather basic. The development of detailed models of 3D nanostructures for the low-temperature Al_2O_3 polymorphs is the subject of further investigations.

Author Contributions: Conceptualization, D.A.Y., V.P.P. and S.V.T.; methodology, D.A.Y., V.P.P. and S.V.T.; software, D.A.Y.; validation, V.P.P. and S.V.T.; investigation, D.A.Y., V.P.P. and S.V.T.; data curation, S.V.T.; writing—original draft preparation, D.A.Y.; writing—review and editing, V.P.P. and S.V.T.; visualization, D.A.Y.; supervision, S.V.T. All authors have read and agreed to the published version of the manuscript.

Data Availability Statement: Not applicable.

Conflicts of Interest: The authors declare no conflict of interest.

References

1. Meephoka, C.; Chaisuk, C.; Samparnpiboon, P.; Praserthdam, P. Effect of phase composition between nano χ- and γ-Al$_2$O$_3$ on Pt/Al$_2$O$_3$ catalyst in CO oxidation. *Catal. Commun.* **2008**, *9*, 546–550. [CrossRef]
2. Chaitree, W.; Jiemsirilers, S.; Mekasuwandumrong, O.; Jongsomjit, B.; Shotipruk, A.; Panpranot, J. Effect of nanocrystalline χ-Al$_2$O$_3$ structure on the catalytic behavior of Co/Al$_2$O$_3$ in CO hydrogenation. *Catal. Today* **2011**, *164*, 302–307. [CrossRef]
3. Macleod, N.; Keel, J.M.; Lambert, R.M. The effects of catalyst aging under industrial conditions: Ethylene oxide conversion over Ag–Cs/α-Al$_2$O$_3$ catalysts. *Catal. Lett.* **2003**, *86*, 51–56. [CrossRef]
4. Busca, G. Chapter Three—Structural, Surface, and Catalytic Properties of Aluminas. *Adv. Catal.* **2014**, *57*, 319–404.
5. Trueba, M.; Trasatti, S.P. γ-Alumina as a Support for Catalysts: A Review of Fundamental Aspects. *Eur. J. Inorg. Chem.* **2005**, *17*, 3393–3403. [CrossRef]
6. Kwak, J.H.; Hu, J.; Mei, D.; Yi, C.-W.; Kim, D.H.; Peden, C.H.F.; Allard, L.F.; Szanyi, J. Coordinatively Unsaturated Al^{3+} Centers as Binding Sites for Active Catalyst Phases of Platinum on γ-Al$_2$O$_3$. *Science* **2009**, *325*, 1670–1673. [CrossRef]
7. Phung, T.K.; Lagazzo, A.; Crespo, M.Á.R.; Escribano, V.S.; Busca, G. A study of commercial transition aluminas and of their catalytic activity in the dehydration of ethanol. *J. Catal.* **2014**, *311*, 102–113. [CrossRef]
8. Nazimov, D.A.; Klimov, O.V.; Trukhan, S.N.; Cherepanova, S.V.; Prosvirin, I.P.; Noskov, A.S. The Effect of Transition Alumina (γ-, η-, χ-Al$_2$O$_3$) on the Activity and Stability of Chromia/Alumina Catalysts. Part I: Model Catalysts and Aging Conditions. *Energy Technol.* **2019**, *7*, 1800735. [CrossRef]
9. Kazakova, M.A.; Vatutina, Y.V.; Prosvirin, I.P.; Gerasimov, E.Y.; Shuvaev, A.V.; Klimov, O.V.; Noskov, A.S.; Kazakov, M.O. Boosting hydrodesulfurization activity of CoMo/Al$_2$O$_3$ catalyst via selective graphitization of alumina surface. *Microporous Mesoporous Mater.* **2021**, *317*, 111008. [CrossRef]
10. Busca, G. The surface of transitional aluminas: A critical review. *Catal. Today* **2014**, *226*, 2–13. [CrossRef]
11. Levin, I.; Brandon, D. Metastable Alumina Polymorphs: Crystal Structures and Transition Sequences. *J. Am. Ceram. Soc.* **1998**, *81*, 1995–2012. [CrossRef]
12. Lippens, B.C.; de Boer, J.H. Study of phase transformations during calcination of aluminum hydroxides by selected area electron diffraction. *Acta Crystallogr.* **1964**, *17*, 1312–1321. [CrossRef]
13. Ushakov, V.A.; Moroz, E.M. Structure of low-temperature γ- and η-Al$_2$O$_3$. *React. Kinet. Catal. Lett.* **1984**, *24*, 113–118. [CrossRef]
14. Paglia, G.; Buckley, C.E.; Rohl, A.L.; Hunter, B.A.; Hart, R.D.; Hanna, J.V.; Byrne, L.T. Tetragonal Structure Model for Boehmite-Derived γ-Alumina. *Phys. Rev. B* **2003**, *68*, 144110. [CrossRef]
15. Samain, L.; Jaworski, A.; Edén, M.; Ladd, D.M.; Seo, D.-K.; Garcia-Garcia, F.J.; Häussermann, U. Structural analysis of highly porous γ-Al$_2$O$_3$. *J. Solid State Chem.* **2014**, *217*, 1–8. [CrossRef]
16. Tsybulya, S.V.; Kryukova, G.N. Nanocrystalline transition aluminas: Nanostructure and features of X-ray powder diffraction patterns of low-temperature Al$_2$O$_3$ polymorphs. *Phys. Rev. B* **2008**, *77*, 024112. [CrossRef]
17. Popescu, C.; Sans, J.A.; Errandonea, D.; Segura, A.; Villanueva, R.; Sapiña, F. Compressibility and Structural Stability of Nanocrystalline TiO$_2$ Anatase Synthesized from Freeze-Dried Precursors. *Inorg. Chem.* **2014**, *53*, 11598–11603. [CrossRef]
18. Daviau, K.; Lee, K.K.M. High-Pressure, High-Temperature Behavior of Silicon Carbide: A Review. *Crystals* **2018**, *8*, 217. [CrossRef]
19. Pakharukova, V.P.; Yatsenko, D.A.; Gerasimov, E.Y.; Shalygin, A.S.; Martyanov, O.N.; Tsybulya, S.V. Coherent 3D nanostructure of γ-Al$_2$O$_3$: Simulation of whole X-ray powder diffraction pattern. *J. Solid State Chem.* **2017**, *246*, 284–292. [CrossRef]
20. Rudolph, M.; Motylenko, M.; Rafaja, D. Structure model of γ-Al$_2$O$_3$ based on planar defects. *IUCrJ* **2019**, *6*, 116–127. [CrossRef]
21. Ivanova, A.S.; Litvak, G.S.; Kryukova, G.N.; Tsybulya, S.V.; Paukshtis, E.A. Real structure of metastable forms of aluminum oxide. *Kinet. Catal.* **2000**, *41*, 122–126. [CrossRef]
22. Kul'ko, E.V.; Ivanova, A.S.; Litvak, G.S.; Kryukova, G.N.; Tsybulya, S.V. Preparation and Microstructural and Textural Characterization of Single-Phase Aluminum Oxides. *Kinet. Catal.* **2004**, *45*, 714–721. [CrossRef]
23. Wolverton, C.; Hass, K.C. Phase stability and structure of spinel-based transition aluminas. *Phys. Rev. B* **2000**, *63*, 024102. [CrossRef]
24. Saalfeld, H.; Mehrota, B.B. Electron-diffraction study of aluminum oxides. *Ber. Dtsch. Keram. Ges.* **1965**, *42*, 161–166.
25. Jayaram, V.; Levi, C.G. The structure of δ-alumina evolved from the melt and the γ → δ transformation. *Acta Metall.* **1989**, *37*, 569–578. [CrossRef]
26. Wang, Y.G.; Bronsveld, P.M.; DeHosson, J.T.M. Ordering of Octahedral Vacancies in Transition Aluminas. *J. Am. Ceram. Soc.* **1998**, *81*, 1655. [CrossRef]
27. Ruberto, C.; Yourdshahyan, Y.; Lundqvist, B.I. Surface properties of metastable alumina: A comparative study of κ- and α-Al$_2$O$_3$. *Phys. Rev. B* **2003**, *67*, 195412. [CrossRef]
28. Prins, R. On the structure of γ-Al$_2$O$_3$. *J. Catal.* **2020**, *392*, 336–346. [CrossRef]
29. Momma, K.; Izumi, F. VESTA 3 for three-dimensional visualization of crystal, volumetric and morphology data. *J. Appl. Cryst.* **2011**, *44*, 1272–1276. [CrossRef]
30. Zhou, R.S.; Snyder, R.L. Structures and transformation mechanisms of the η, γ and θ transition aluminas. *Acta Crystallogr. Sect. B* **1991**, *47*, 617–630. [CrossRef]
31. Drits, V.A.; Tchoubar, C. *X-ray Diffraction by Disordered Lamellar Structures*; Springer: Berlin/Heidelberg, Germany, 1990; p. 371.
32. Cherepanova, S.V.; Tsybulya, S.V. Simulation of X-ray powder diffraction patterns for one-dimensionally disordered crystals. *Mat. Sci. Forum* **2004**, *443–444*, 87–90. [CrossRef]

33.   Debye, P. Zerstreung von Röntgenstrahlen. *Ann. Physik.* **1915**, *351*, 809–823. [CrossRef]
34.   Tsybulya, S.V.; Yatsenko, D.A. X-ray diffraction analysis of ultradisperse systems: The Debye formula. *J. Struct. Chem.* **2012**, *53*, S150–S165. [CrossRef]
35.   Gelisio, L.; Scardi, P. 100 years of Debye's scattering equation. *Acta Crystallogr. Sect. A* **2016**, *72*, 608–620. [CrossRef] [PubMed]
36.   Yatsenko, D.; Tsybulya, S. DIANNA (Diffraction Analysis of Nanopowders)—A software for structural analysis of nanosized powders. *Z. Kristallogr. Cryst. Mater.* **2018**, *233*, 61–66. [CrossRef]
37.   Wojdyr, M. Fityk: A general-purpose peak fitting program. *J. Appl. Cryst.* **2010**, *43*, 1126–1128. [CrossRef]
38.   Scherrer, P. Bestimmung der Grösse und der inneren Struktur von Kolloidteilchen mittels Röntgenstrahlen. *Nach. Gesell. Wissen. Göttingen* **1918**, *2*, 98–100. [CrossRef]
39.   Shirai, T.; Watanabe, H.; Fuji, M.; Takahashi, M. Structural Properties and Surface Characteristics on Aluminum Oxide Powders. 2009, 9, 23–31. *Annu. Rep. Ceram. Res. Lab. Nagoya Inst. Technol.* **2009**, *9*, 23–31.